

Improved Light Soaking and Thermal Stability of Organic Solar Cells by Robust Interfacial Modification

Mwende Mbilo, Muhammad Haris, Du Hyeon Ryu, Julius Mwakondo Mwabora, Robinson Juma Musembi, Seungjin Lee, Chang Eun Song,* and Won Suk Shin*

The most widely used material in electron transport layers (ETL) of inverted organic solar cells (iOSCs) is zinc oxide (ZnO). However, the brittleness, inorganic nature, surface defects, and photocatalytic activity of ZnO lead to poor stability in iOSCs. Herein, the light-soaking and thermal stability of iOSCs are substantially improved by modifying ZnO surface with polyurethane diacrylate (SAR) or urethane acrylate (OCS)-based ultraviolet (UV) resins. The UV resins significantly reduce the energy barrier, suppress surface defects, and improve interfacial contact between ZnO ETL and the organic photoactive layer. Notably, the SAR and OCS resins mitigate the photocatalytic activity of ZnO, electrical leakage, and interfacial resistance during photoaging of OSCs. As a result, iOSCs based on modified ZnOs retain over 80% of initial efficiency under 1 sun illumination for light soaking 1000 h. Furthermore, SAR and OCS resins on ZnO surfaces form a robust crosslinked network with excellent solvent resistant properties, which result in enhanced thermal stability. These results reveal that this simple and effective approach is a promising procedure to fabricate high-performance iOSCs.

owing to the realization of high power conversion efficiencies (PCEs) surpassing 19%.^[1–3] However, insufficient long-term stability of OSCs remains a major obstacle to their commercial applicability.^[4] Ideally, high-efficiency OSCs should present consistent performance over lifetime operation. This has not been the case due to degradation upon exposure to environmental changes.^[5] The instability of OSCs may result from extrinsic factors such as mechanical stress, light, heat, moisture, and oxygen or from intrinsic factors including unstable bulk heterojunction (BHJ) morphology and diffusion of metal electrodes and buffer layers to the photoactive systems.^[6] Thus far, most investigations have emphasized improving the stability of OSCs based on stable BHJ morphological optimization.^[7–9] It noteworthy that charge transport interlayers (CTIs) also play a role in realizing highly stable OSCs.^[10]

1. Introduction


Recently, organic solar cells (OSCs) based on nonfullerene acceptors (NFAs) have attracted considerable research interest

A variety of materials have been synthesized and applied as CTIs in OSCs, including polymers, small molecules, composites, hybrids, metals, metal salts, complexes, and metal oxides.^[11–16] In inverted NFA-based OSCs, zinc oxide (ZnO) is commonly used as an electron transport layer (ETL) owing to its easy solution processing, appropriate energy levels, low cost, excellent visible transparency, and high electron mobility.^[17,18] However, ZnO ETL suffers from various shortcomings that must be resolved to achieve high- and stable-efficiency OSCs. Typically, ZnO is brittle in nature, which makes its interface with photoactive films prone to delamination and punctures under environmental stress.^[19] The inorganic nature of ZnO also results in interfacial mismatch of surface energies with the organic photoactive layer.^[20] This leads to interfacial defects, which affect the molecular ordering and aggregation of the photoactive materials, causing OSC instability.^[20] Moreover, ZnO is a renowned photocatalyst of organic compounds upon UV light illumination.^[21–23] ZnO absorbs UV light and generates electron–hole pairs, which react with the oxygen and water absorbed on the surface to form reactive oxygen species (ROS), called superoxide anions and hydroxide radicals.^[24–28] These ROS have been reported to decompose NFAs, leading to instability issues in OSCs.^[29] It has also been reported that various surface defects including dangling bonds, hydroxyl groups, and oxygen vacancies exist on the surface of solution-processed ZnO.^[30,31] These surface defects act as photogenerated charge recombination centers, resulting

M. Mbilo, J. M. Mwabora, R. J. Musembi
Department of Physics
Faculty of Science and Technology
University of Nairobi (UoN)
P.O. Box 30197-00100, Nairobi 00100, Kenya

M. Mbilo, M. Haris, D. H. Ryu, S. Lee, C. E. Song, W. S. Shin
Advanced Energy Materials Research Center
Korea Research Institute of Chemical Technology (KRICT)
Daejeon 34114, Republic of Korea
E-mail: songce@kRICT.re.kr; shinws@kRICT.re.kr

M. Haris, C. E. Song, W. S. Shin
Advanced Materials and Chemical Engineering
University of Science and Technology (UST)
Daejeon 34113, Republic of Korea

 The ORCID identification number(s) for the author(s) of this article can be found under <https://doi.org/10.1002/aesr.202300210>.

© 2024 The Authors. Advanced Energy and Sustainability Research published by Wiley-VCH GmbH. This is an open access article under the terms of the Creative Commons Attribution License, which permits use, distribution and reproduction in any medium, provided the original work is properly cited.

DOI: 10.1002/aesr.202300210

in limited efficiency and stability of OSCs. Replacement of ZnO with photocatalytic-inert materials and insertion of suitable interfacial layers between ZnO and organic photoactive film have been reported as strategies to address these instability issues.^[32–36]

Although efforts to enhance the stability of OSCs reported this far have significantly contributed to organic photovoltaic technology, some studies have employed ETLs processed at high temperatures for long times and from halogenated solvents. Thermal stress can distort plastic substrates, hindering their flexibility, and reduce the conductivity of indium tin oxide (ITO) electrodes.^[37,38] In addition, the use of halogenated solvents such as chloroform and chlorobenzene can lead to health and environmental threats.^[39]

Furthermore, a number of photostability tests were conducted under 1 sun, simulated by a light emitting diode light source, which has a weaker spectral irradiance in the UV light region compared to those of metal halide sources, bringing forth spectral irradiance nonuniformity issues in photostability tests.^[40] Also, for other reports, thermal stability tests were carried out in nitrogen-filled gloveboxes in the dark where humidity is very low (<20%). In the absence of oxygen and moisture, it is likely that this stability test is not reasonable for thermally stable OSCs.

We therefore provide a simple and effective approach to enhance the efficiency and stability of inverted NFA-based OSCs utilizing the crosslinking strategy. Herein, commercially available diacrylate and acrylate-based UV resins, referred to as SAR and OCS, respectively, were employed to mitigate the photocatalytic effect and surface defects of ZnO. Unlike reported CTIs, the SAR and OCS resins used in this study were processed from nonhalogenated solvent (2-methoxyethanol, 2-ME) under ambient conditions and were crosslinked on the ZnO surface

under UV lamp illumination within 5 min. The SAR and OCS resins on the ZnO surface demonstrated a high solvent resistance characteristic to solvent washing, which is beneficial for forming the robust crosslinked networks. The ETL of SAR or OCS resins crosslinked on the ZnO surface substantially reduced the shunt path and leakage current, as well as providing improved interfacial contacts and energy-level alignment between ZnO and the photoactive layer. This phenomenon consequently led to highly enhanced photovoltaic parameters with superior light soaking and thermal stability in OSCs.

2. Results and Discussion

In this study, SAR and OCS UV resins based on urethane acrylate with viscosities of 51 400 and 3720 mPa s, respectively, were utilized. The device architecture and chemical structures of the SAR and OCS are shown in **Figure 1a**. The presence of acrylate groups in the chemical structures endowed the resins with crosslinking capability. The resins possess reactive chemical groups, mainly amines and isocyanate, which can react directly with reactive hydroxyl groups on the ZnO surface, yielding functionalization effects such as defect passivation.^[41,42] The amine groups can further form an interfacial dipole between ZnO and the photoactive layer, thus tuning the work function (WF).^[43] The UV-vis absorption spectra of neat ZnO, SAR, and OCS were measured and the corresponding bandgaps were obtained from the Tauc plot, as shown in Figure S1, Supporting Information. The UV resins showed weak absorption in the UV-visible region of 300–800 nm and wide bandgaps (3.95 and 3.88 eV for SAR and OCS, respectively), compared to those of bare ZnO, showing strong absorption in the UV region (300–400 nm) with a bandgap of 3.28 eV. Due to the wider bandgaps, the UV resins are unlikely

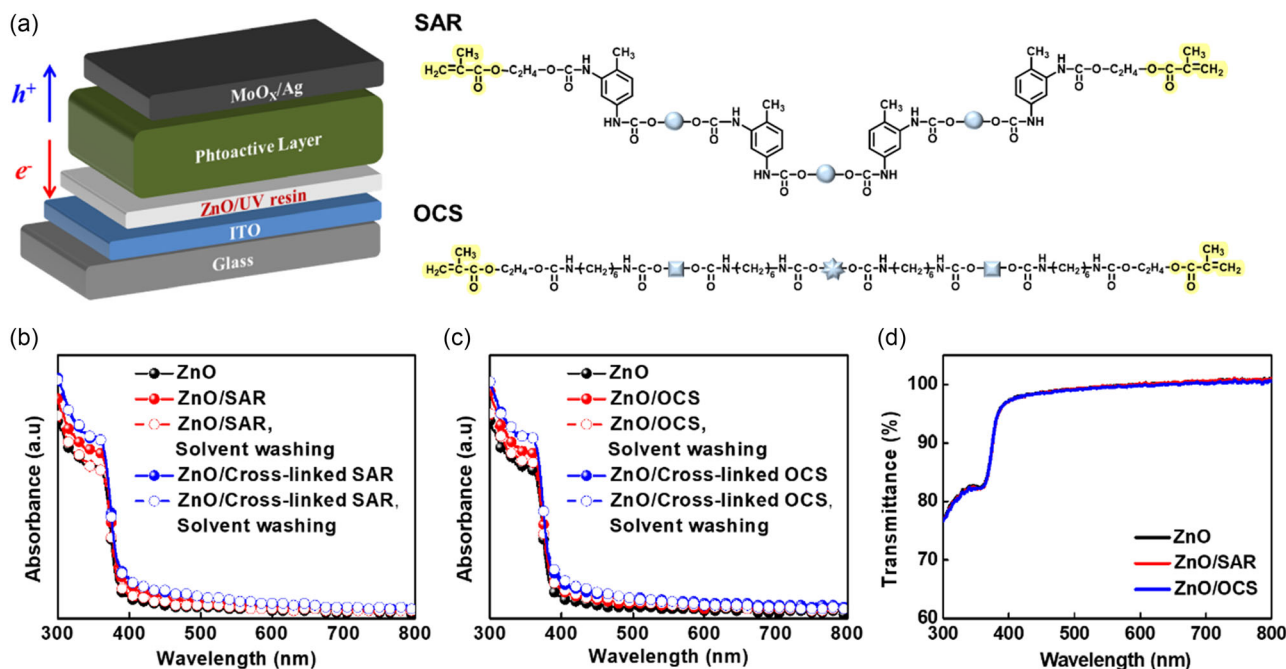


Figure 1. a) Inverted device architecture of OSCs and chemical structures of SAR and OCS UV resins. Optical absorption spectra of fresh and crosslinked b) ZnO/SAR and c) ZnO/OCS ETL before and after solvent washing with 2-ME. d) Transmission spectra of ZnO, ZnO/SAR, and ZnO/OCS ETL.

to absorb light in the AM1.5 irradiation range,^[23] hence, it is anticipated that modification of the ZnO surface with UV resins will substantially reduce the photocatalytic effect and not interrupt the light absorption of the photoactive layer.

The solvent resistance properties were determined according to the reported literature^[44,45] by monitoring the changes in the light absorption intensities of the crosslinked resins on ZnO surface after washing with processing solvent. Herein, both fresh and crosslinked films were washed with 2-ME solvent by spin coating at 5000 rpm for 60 s twice to demonstrate the degree of crosslinking. As shown in Figure 1b,c, the intensity of absorbance of the uncrosslinked films decreased to nearly that of bare ZnO film, while the light absorption intensity of the crosslinked films remained unchanged after solvent washing. These results demonstrate that the crosslinked resins exhibit high solvent-resistant properties, beneficial for the formation of a robust interface as well as resistance to interfacial erosion between ZnO and the photoactive layer due to various solution processing techniques. Slightly enhanced absorbance in the UV region was observed in the case of modified ZnO with SAR and OCS resins, whereas there was no obvious optical transmittance loss in the visible light region, as shown in Figure 1d.

The wettability of the ZnO surface without and with UV resins was studied by measuring the contact angles in water and diiodomethane (DIM), with results displayed in Figure S2, Supporting Information. The corresponding surface free energy (γ) was calculated according to the Owen–Wendt method, with results tabulated in Table S1, Supporting Information.^[46] The contact angles of water and DIM on ZnO are 34.9° and 26.8°, respectively, and the calculated surface energy is 64.48 mJ m⁻². ZnO/SAR exhibits water and DIM contact angles of 58.4° and 29.0°, respectively, and a calculated surface energy of 51.95 mJ m⁻². Similarly, the contact angles of water and DIM on modified ZnO with OCS were 71.2° and 26.0°, respectively,

and the corresponding surface energy was 47.93 mJ m⁻². For the PM6:Y6-BO BHI film (molecular structures are depicted in Figure S3, Supporting Information), the water and DIM contact angles were 104.3° and 58.6°, respectively, and the calculated surface energy was 29.74 mJ m⁻². Compared with pristine ZnO, ZnO/SAR, and ZnO/OCS possess hydrophobicity and surface energy more similar to those of the organic photoactive layer, whose qualities should decrease the mechanical driving force for delamination and improve the interfacial contact between the ETLs and the organic photoactive layer.^[19]

It is well known that the presence of interfacial modification in OSCs affects the WF of electrodes, thus providing Ohmic contact at the electrodes. Therefore, we measured the WFs of pristine ZnO, ZnO/SAR, and ZnO/OCS using ultraviolet photoelectron spectroscopy (UPS), with results shown in Figure S4, Supporting Information. The WF values of neat ZnO, ZnO/SAR, and ZnO/OCS were calculated and found to be \approx 3.83, 3.80, and 3.71 eV, respectively. The WF of modified ZnO decreased moderately compared with that of bare ZnO, which can facilitate electron extraction and block hole transportation to the cathode through improved Ohmic contact due to the generation of amine-induced dipole moments, which line up in a direction pointing out from the ZnO surface. This phenomenon has frequently been used to explain the enhanced open-circuit voltage (V_{OC}) in other studies dealing with interfacial modification of buffer layers. Actually, our inverted OSCs with SAR and OCS showed greater V_{OC} values, in line with the upshifted WF of the modified ZnO, maximizing the obtainable V_{OC} .^[47]

To gain insight into the chemical states of the ZnO surface before and after crosslinking of UV resins, X-ray photoelectron spectroscopy (XPS) measurements were carried out. **Figure 2** shows the variation of the core-level XPS spectra of Zn 2p_{3/2} and O 1s for the ZnO surfaces. The binding energy of the Zn 2p_{3/2} peak for pristine ZnO as prepared on ITO/glass

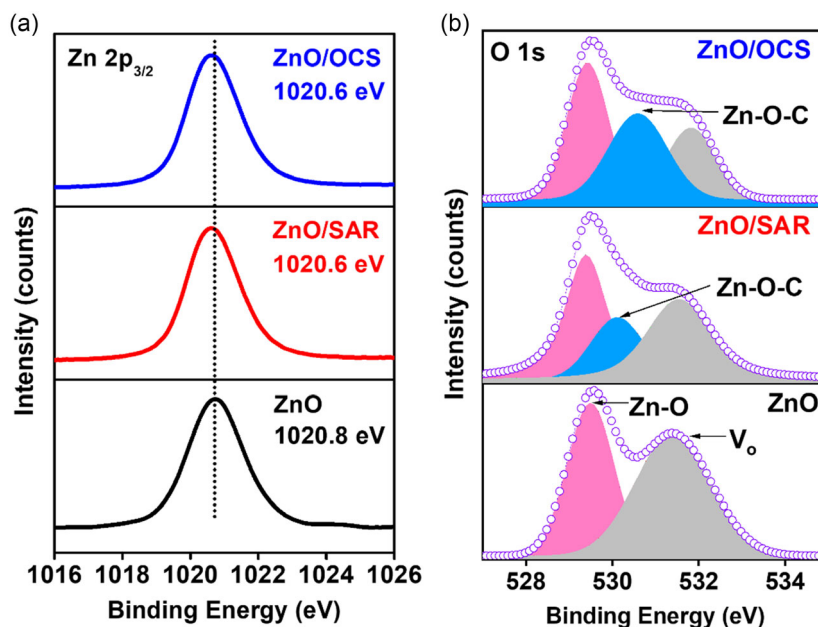


Figure 2. XPS spectra for bare ZnO, ZnO/SAR, and ZnO/OCS on the ITO substrate. a) Zn 2p_{3/2} and b) O 1s core level.

substrate was nearly in agreement with the reported values,^[31] corresponding to Zn–O bonds of the ZnO bulk phase with plenty of exposed surfaces. When the ZnO surface was cross-linked by UV resins, the maximum peak position of Zn 2p_{3/2} shifted significantly (by about 0.2 eV) toward a lower binding energy. This implies that Zn atoms were less exposed to the surface and bound to more surrounding O atoms; this binding is ascribed to electron transfer from crosslinked UV resins (in accordance with UPS results). The XPS spectrum of the O 1s core level resolved into two components for the bare ZnO surface, as shown in **Figure 3b**. The peak with the lowest binding energy is generally assigned to O²⁻ ions surrounded by Zn atoms of ZnO crystals with a normal wurzite structure, that is, bulk-phase oxygen (Zn–O). In contrast, the other peak with highest binding energy can be attributed to O²⁻ ions in the oxygen vacant sites (V_O) of the ZnO matrix. After modification of the ZnO surface with UV resins, ZnO/SAR and ZnO/OCS revealed a new peak located between the Zn–O and V_O peaks. This peak is attributed to the formation of chemical bonding (Zn–O–C), in which the carbon atom from the carbonyl group (C=O) of the UV resins replaces the hydrogen of the hydroxyl (–OH) on the ZnO surface.^[31,48] It was thus found that analysis of the intensity ratio of the V_O to Zn–O peaks showed a decrease from 0.81 for neat ZnO surface to 0.64 and 0.53 for ZnO/SAR and ZnO/OCS, respectively, demonstrating that the surface defects on bare ZnO surface were considerably suppressed after UV resin modification.

Further study on surface defect passivation of neat ZnO was conducted by steady-state photoluminescence (PL) spectroscopy, with results presented in Figure S5, Supporting Information. The PL spectra of pristine ZnO exhibited two major emission peaks. The near-band-edge strong emission peak at ≈393 nm

can be ascribed to exciton recombination in ZnO, while the low-intensity broad emission peak in the visible region arose from the surface defects on ZnO.^[30,31,49] The ratios of the near-band-edge and the visible region PL intensity were 0.92, 0.89, and 0.88 for ZnO, ZnO/SAR, and ZnO/OCS, respectively. A decrease in the fluorescence intensity ratio after modification of the ZnO surface by UV resins implied effectively suppressed surface defects, which is in good agreement with previous XPS results (Figure 2).

To evaluate the ETL-dependent device performance, we fabricated OSCs with inverted device architecture of ITO/ETL/PM6:Y6-BO/MoO₃/Ag, according to the procedure described in the Supporting Information. The best current density–voltage (*J*–*V*) characteristics and external quantum efficiency (EQE) spectra of OSCs without and with UV resins under illumination of AM1.5G, 100 mW cm⁻² are displayed in Figure 3a,b; the corresponding photovoltaic parameters are summarized in **Table 1**. Clearly, the photovoltaic performances of the OSCs were substantially enhanced when modified ZnO ETLs were used instead of pristine ZnO. The OSC based on PM6:Y6-BO with bare ZnO ETL showed a PCE value of 14.2%, with a V_{OC} of 0.80 V, a short-circuit current density (*J*_{SC}) of 25.2 mA cm⁻², and fill factor (FF) of 70.0%. In the case of the OSC with ZnO/SAR, the PCE substantially improved to yield a PCE of 16.1%, with a V_{OC} of 0.83 V, a *J*_{SC} of 26.0 mA cm⁻², and FF of 74.5%. In addition, the inverted OSC fabricated with ZnO/OCS yielded a photovoltaic performance of V_{OC} = 0.83 V, *J*_{SC} = 26.0 mA cm⁻², and FF = 74.2% (PCE = 16.1%). The overall enhanced PCE values of devices incorporating crosslinked ZnO with UV resins are apparently due to simultaneous increases in the three photovoltaic parameters, (V_{OC}, *J*_{SC}, and FF) relative to those without the modification. Integrating the product of the measured EQE under photon

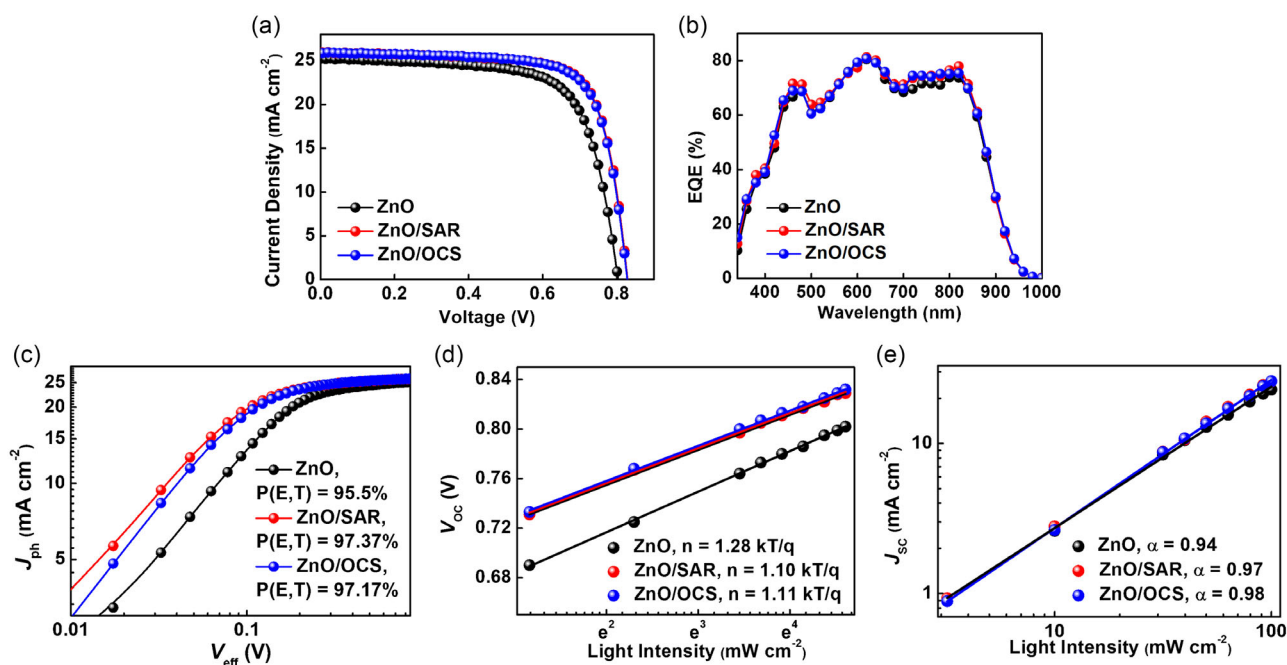


Figure 3. a) Best *J*–*V* characteristics of optimized OSCs under illumination of 100 mW cm⁻² and b) EQE curves of the corresponding devices. c) *J*_{ph}–*V*_{eff} characteristics of OSCs based on different ETLs. Dependence of d) V_{OC} and e) *J*_{SC} on incident light intensity of OSCs with different ETLs.

Table 1. Summary of the photovoltaic parameters of inverted BHJ OSCs based on different ETLs under the illumination of AM 1.5G, 100 mW cm⁻².

| ETL | V _{OC} [V] | J _{SC} [mA cm ⁻²] | J _{SC} ^{cal} [mA cm ⁻²] ^{a)} | FF [%] | PCE [%] |
|---------|------------------------------------|--|---|------------------------------------|------------------------------------|
| ZnO | 0.80 (0.79 ± 0.1) ^{b)} | 25.2 (25.1 ± 0.2) ^{b)} | 24.2 | 70.0 (69.7 ± 0.4) ^{b)} | 14.2 (14.0 ± 0.2) ^{b)} |
| ZnO/SAR | 0.83 (0.83 ± 0.1) ^{b)} | 26.0 (25.8 ± 0.2) ^{b)} | 25.0 | 74.5 (74.2 ± 0.2) ^{b)} | 16.1 (16.0 ± 0.1) ^{b)} |
| ZnO/OCS | 0.83 (0.82 ± 0.1) ^{b)} | 26.0 (25.9 ± 0.1) ^{b)} | 25.0 | 74.2 (74.0 ± 0.3) ^{b)} | 16.1 (16.0 ± 0.1) ^{b)} |

^{a)}The integrated current density values calculated from the EQE spectra; ^{b)}In-parentheses, statistical values obtained from average of over six independent devices.

flux density of the AM 1.5G solar spectrum yielded J_{SC}s of 24.2, 25.0, and 25.0 mA cm⁻² for bare ZnO, ZnO/SAR, and ZnO/OCS ETL, respectively, which were consistent, within experimental errors of ≈5%, with the J_{SC} value measured under AM 1.5G conditions. Enhancement of the EQE response in the wide region of 350–900 nm after modifying the ZnO surface with the SAR and OCS resins implied improved photon-to-electron conversion efficiency, which is one of the reasons for the enhanced J_{SC} value. Interestingly, OSCs based on UV crosslinking resins exhibit improved V_{OC} compared to that of bare ZnO-based device, which is attributed to mitigated interfacial defects and well-aligned energy level between the ZnO and photoactive layer, leading to the minimized energy loss.

To determine the reason for the improved photovoltaic performance in resin-employing OSCs, electron-only devices with ITO/ETL/PM6:Y6-BO/ZnO/Ag architecture were fabricated. The electron transport properties of OSCs with pristine ZnO and crosslinked ZnO were evaluated by measuring the electron mobility (μ_e) in the space-charge-limited current (SCLC) regime (Figure S6, Supporting Information) using the Mott-Gurney relation of μ_e = 8J_{SCLC}L³/9V²εε₀,^[50,51] where J/V² is the slope of current density J_{SCLC} versus voltage (V = V_{appl} - V_{bi} - V_r, where V_{appl} is the applied voltage, V_{bi} reveals the built-in potential determined by electrode WF difference, and V_r indicates the voltage drop, which occurred due to contact resistance and series resistance across the electrodes) in the child's region, L is the thickness of the photoactive film, ε is relative dielectric constant of the photoactive layer, and ε₀ is the dielectric constant in vacuum. The SCLC device based on pristine ZnO showed a low μ_e of 4.37 × 10⁻⁴ cm² V⁻¹ S⁻¹. In contrast, the μ_e values of the ZnO/SAR- and ZnO/OCS-based device increased to 5.53 × 10⁻⁴ and 5.70 × 10⁻⁴ cm² V⁻¹ S⁻¹, respectively. The enhancement of μ_e values due to UV resin modification of ZnO surface reveals that the electron transport capability in OSCs improved, leading to higher values of FF and J_{SC}.

The enhanced electron transport and extraction in modified ZnO devices were further supported by the dependence of photocurrent density J_{ph} (J_{ph} = J_{light} - J_{dark}, where J_{light} and J_{dark} are the current density under 1.5 AM illumination and darkness, respectively) versus effective voltage V_{eff} (V_{eff} = V_O - V_{appl}, where V_O is the voltage at J_{ph} equal to zero and V_{appl} is the applied voltage) characteristics (Figure 3c).^[52] The exciton dissociation probability, P(E,T), in OSCs was obtained from the normalized value of J_{ph} with respect to the saturated current density

(J_{sat}) (J_{ph}/J_{sat}) under short-circuit conditions. P(E,T) values, which are related to the charge transfer efficiency, were found to be 95.5%, 97.4%, and 97.2%, for devices incorporating ZnO, ZnO/SAR, and ZnO/OCS, respectively. The enhanced P(E,T) of the crosslinked OSCs implied that the morphology of photoactive films can be readily altered by surface properties of ETLs underneath. As shown in Figure S7, Supporting Information, the uniform and homogeneous morphology of PM6:Y6-BO films coated on ZnO/SAR and ZnO/OCS with smaller root mean square roughness (RMS) compared with that of neat ZnO/PM6:Y6-BO film, which resulted in the improved P(E,T) values.

Additionally, the charge carrier recombination properties were investigated by evaluating the dependence of the values J_{SC} and V_{OC} on the incident light intensity (P_{light}). The bimolecular charge recombination is termed dominant, when the slope of V_{OC} versus P_{light} (n) approaches kT/q,^[53] while the trap-assisted charge recombination dominates when the slope of V_{OC} versus P_{light} (n) approaches 2 kT/q.^[54] Here, k is the Boltzmann constant, T is absolute temperature, and q is elementary charge. As depicted in Figure 3d, higher values of n = 1.28 kT/q in bare ZnO-based OSCs led to more trap-assisted charge recombination compared to the case of OSCs with ZnO modified by SAR (n = 1.10 kT/q) and OCS (n = 1.11 kT/q). The charge recombination status in these OSCs is also investigated via the dependence of J_{SC} on the incident light intensity (Figure 3e). The power law equation J_{SC} ∝ (P_{light})^α is used to describe the correlation between J_{SC} and P_{light}, where α is an exponential factor. A weak bimolecular recombination is indicated by an α value close to 1. The α values for the OSCs with bare ZnO, ZnO/SAR, and ZnO/OCS range from 0.94, 0.97, and 0.98, respectively. Thus, the crosslinking of UV resins on ZnO surface benefits from the substantially reduced trap-assisted and bimolecular recombination, leading to improved photovoltaic performance of OSCs.

Considering the lower enthalpy of the ZnO/Y6-BO interface in comparison to that of the ZnO/PM6 interface, Y6-BO NFAs are expected to preferentially distribute on the ZnO surface, making them prone to immediate attack by ROS generated by ZnO. Therefore, the UV-vis absorption spectra were measured for UV light stability by monitoring the photochemical degradation behavior of Y6-BO NFAs coated on ZnO under UV lamp (365 nm, 8 W) illumination (Figure 4a–c). The evolution of the Y6-BO absorption intensity peaks at ≈840 nm was monitored with respect to changes in the irradiation time, as illustrated

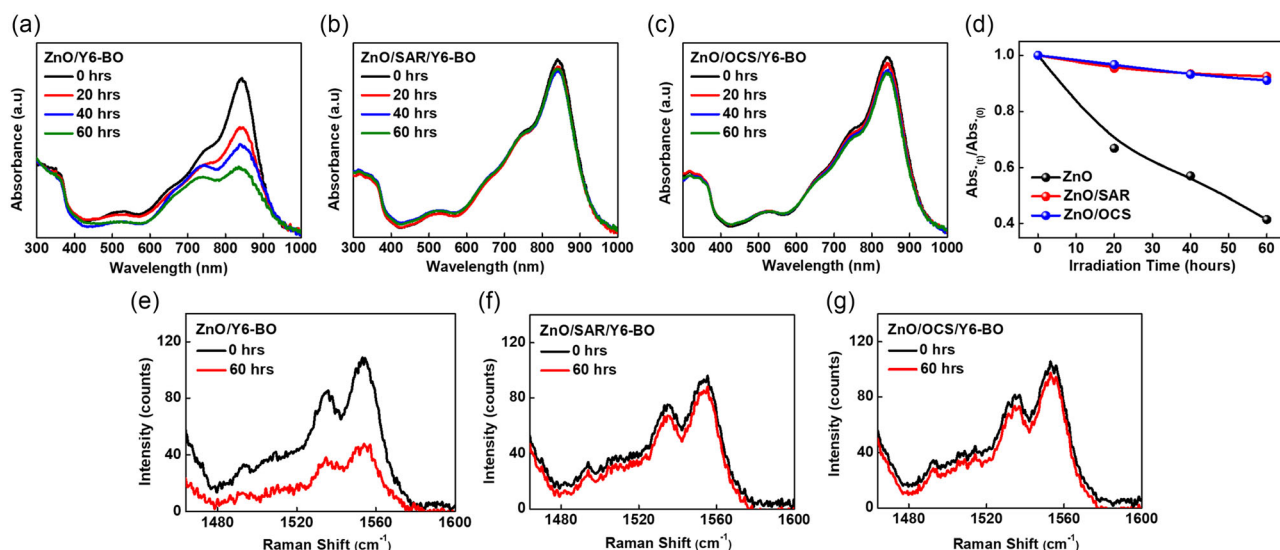


Figure 4. The UV-vis absorption spectra of Y6-BO coated on a) ZnO, b) ZnO/SAR, and c) ZnO/OCS ETL as a function of UV lamp illumination time. d) Comparison of the changes in the absorption intensity of Y6-BO coated on various ETLs as a function of UV lamp irradiation time. The Raman spectra of fresh and photoaged Y6-BO on e) ZnO, f) ZnO/SAR, and g) ZnO/OCS ETL.

in Figure 4d. The absorption intensity of Y6-BO on pristine ZnO film decreased dramatically within 60 h of UV irradiation. On the contrary, Y6-BO on the ZnO/SAR and ZnO/OCS showed a slower absorption intensity decay trend. These results indicate that the UV resins with wide bandgaps shielded the photocatalytic effect of ZnO from direct contact with the photoactive layer, thus mitigating the photodegradation of Y6-BO. This is speculated to be the reason that the UV light stability of Y6-BO on the modified ZnO surface improved compared to that on bare ZnO.

The UV light stability of Y6-BO coated on ZnO-based ETLs was further investigated using Raman spectroscopy, according to processes in the literature.^[32] As shown in Figure 4e–g, the peak in the Raman spectra at 1553 cm^{-1} as a result of the C=C bond joining the donor to acceptor moieties in Y6-BO NFA were largely quenched after 60 h UV irradiation for the case of bare ZnO film. In contrast, the intensity peak of the C=C bond of Y6-BO on ZnO films modified with SAR and OCS exhibited a substantially slower decay, which is in accordance with the UV-vis spectroscopy results, which showed that the photocatalytic effect of ZnO was effectively mitigated by UV resin modification. When the UV lamp is replaced with a xenon arc source, the Y6-BO film on bare ZnO is also unstable compared to that based on UV crosslinked resins with changed absorbance (Figure S8, Supporting Information). This suggests that the degradation of Y6-BO by photocatalytic effect of ZnO is attributed to the UV spectral region of the AM1.5 spectrum. Consequently, the ZnO/UV resin ETLs are expected to deliver exceptional photostability for the inverted OSCs.

In addition to the device efficiency, the light-soaking stability was investigated by monitoring the PCE evolution of glass-to-glass-encapsulated OSCs based on bare and modified ZnO ETLs under continuous 1 sun illumination (100 mW cm^{-2}) using metal halide light source. Figure S9, Supporting Information, shows the light spectrum of metal halide lamp used

for the photodegradation test. Optimization of the light soaking stability based on the various UV resin concentrations was carried out, as depicted in Figure S10, Supporting Information. With 0.52 wt% of UV resin, the electrical current leakage in OSCs was found to reach its lowest level and highest photostability performance after 90 h. The light-soaking test was further investigated for up to 1000 h under the optimized conditions; decay curves of inverted OSCs without and with UV resin modification are shown in Figure 5a. Performance of UV resin-processed OSCs with SAR and OCS remained remarkably stable, with decreases in efficiency of only 19% over a period of 1000 h under continuous 1 sun light exposure. In sharp contrast, the control device decayed very rapidly, showing a 44% decline in initial PCE. These results were in agreement with improved UV light stability for OSCs with SAR- or OCS-based interfacial modification. The main contribution to the stable performance observed in the modified devices during the photostability test can be attributed to the enhanced values of FF and J_{SC} (Figure S11 and Table S2–S4, Supporting Information). Changes of dark current behavior in OSCs before and after the photostability test were also investigated, as shown in Figure 5b. It is important to mention that the origin of the dark current density (J_{dark}) can be mainly explained by bimolecular charge recombination at the interface, which is directly determined by the FF values of the relevant devices. Compared to the control OSC, leakage or dark currents were significantly suppressed in the fresh OSCs with crosslinked UV resins, leading to improved diode characteristics and rectification ratios (current density at 2 V divided by the current density at -2 V) of the devices. More encouragingly, the dark characteristics of the photoaging devices with modified ZnO surface were similar to those of fresh OSCs. In contrast, the neat ZnO-based device exhibited low shunt resistances, high value of J_{dark} , and reduced rectification of diodes after the photostability test.

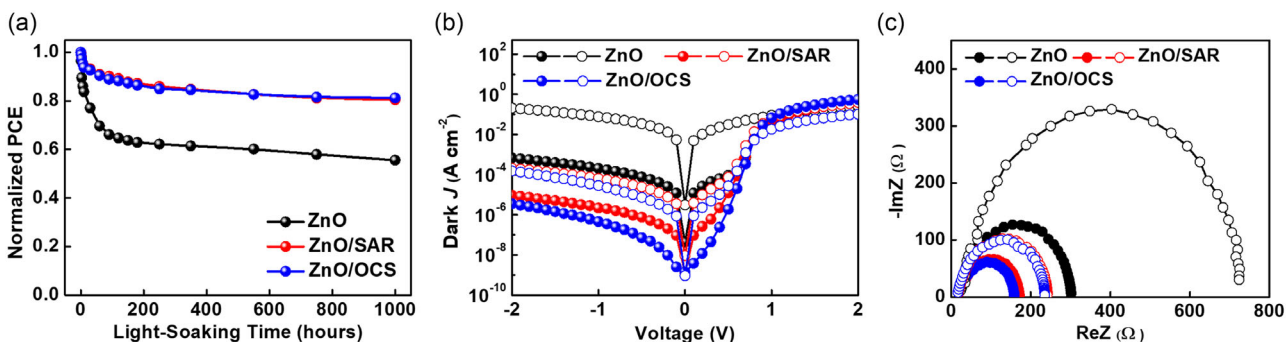


Figure 5. a) Normalized PCE decay curves of OSCs with different ETLs as a function of light-soaking time and b) corresponding dark J - V curves before (filled symbols) and after (blank symbols) photostability test. c) EIS spectra of OSCs with different ETLs before (filled symbols) and after (blank symbols) light soaking for 100 h.

To further understand the reason for the enhanced light-soaking stability, we subjected the unencapsulated OSCs to light-soaking stress for 100 h and then measured the exciton dissociation probability and charge recombination property, as shown in Figure S12, Supporting Information. After the photostability test, the pristine ZnO-based OSCs showed a substantial 10.0% decrease in exciton dissociation probability, while the OSCs based on ZnO/SAR and ZnO/OCS ETL exhibited only 2.8% and 1.9% declines. Similarly, logarithmic dependence of V_{OC} on incident P_{light} with slope increments of 0.49, 0.16, and 0.10 kT/q for OSCs with ZnO, ZnO/SAR, and ZnO/OCS ETL, respectively, was observed, compared with those of fresh devices. Furthermore, electrochemical impedance spectroscopy (EIS) was used to determine changes in charge transport resistance of unencapsulated OSCs based on various ETLs before and after light-soaking test for 100 h (Figure 5c). The equivalent circuit model used to fit the EIS is presented in Figure S13, Supporting Information. Comparisons of the series resistance before and after photoaging for 100 h revealed that OSCs based on ZnO/SAR (3.8 Ω) and ZnO/OCS (2.8 Ω) had subtle variations in charge transport resistance compared to that of the control device (12.4 Ω). From the above results, we can deduce that interface charge accumulation between modified ZnO ETLs and the photoactive layer was effectively reduced compared to the case of OSC with bare ZnO ETL, leading to the remarkable

improvement of light-soaking stability in OSCs based on modified ZnO ETLs. To the best of our knowledge, among OSCs with ZnO ETL, this study presents the best photostability under metal halide light source 1 sun illumination. (Table S5, Supporting Information).

Apart from the photostability, the thermal stability in OSCs is also critical for practical applications of this emerging technology. We conducted a thermal-stress stability test for PM6:Y6-BO-based unencapsulated OSCs without and with SAR or OCS UV resin on a hot plate in ambient air at 120 $^{\circ}\text{C}$ /55 \approx 68% relative humidity for 200 h. Dependences of PCE on annealing time of the three OSCs based on various ETLs and corresponding changes of the J - V curves before and after the thermal stress are depicted in Figure 6a,b. As shown in Figure 6a, the percentages of the initial PCE losses were 42%, 27%, and 22% for devices with bare ZnO, ZnO/SAR, and ZnO/OCS ETL, respectively. The performance drop is more severe for the control OSC than that for the devices with ZnO modification. The photovoltaic parameter that contributed most to the stable performance of OSCs under thermal stress was FF (Table S6–S8, Supporting Information). These results indicate that crosslinked ZnO with UV resins may have played a significant role in mitigating thermally induced interfacial charge recombination and morphological degradation.

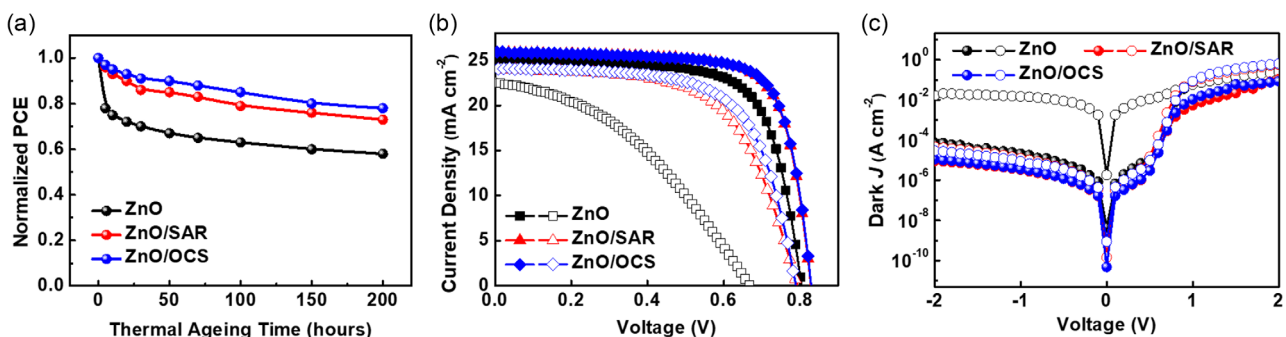


Figure 6. Thermal stability characteristic. a) Normalized PCE decay curves as a function of thermal stress time at 120 $^{\circ}\text{C}$ for unencapsulated OSCs with different ETLs. b) Best J - V curves under (b) 1.5 AM illumination and c) dark OSCs with different ETLs before (filled symbols) and after (blank symbols) thermal stress test for 200 h.

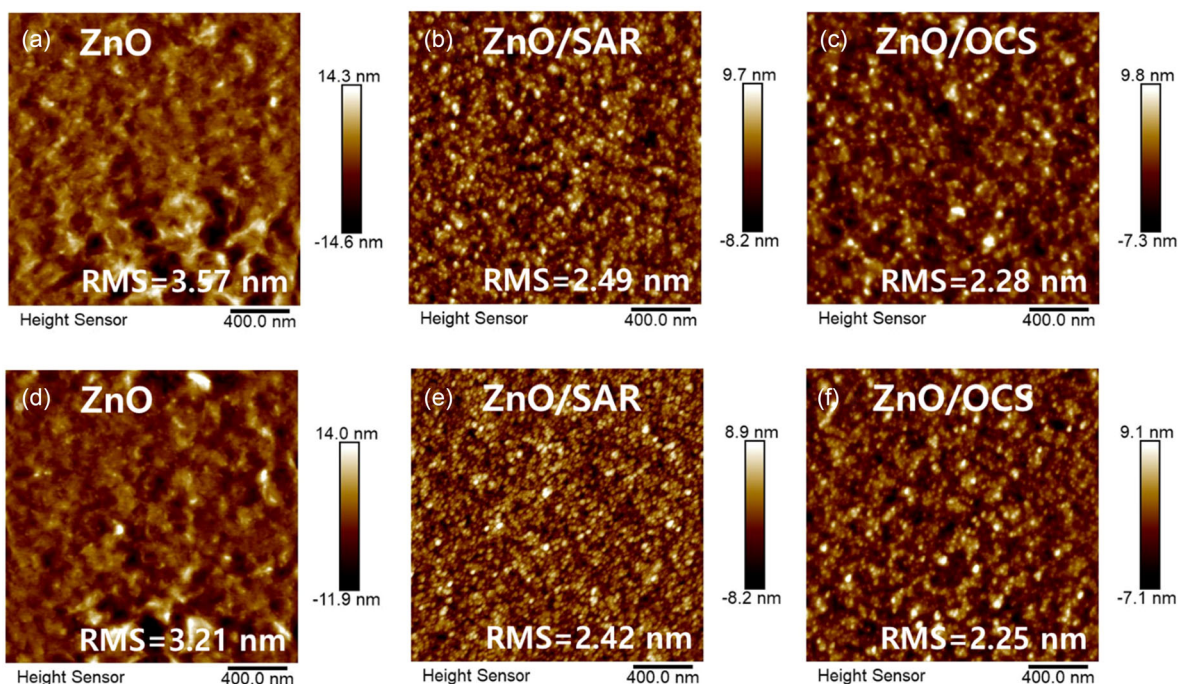


Figure 7. AFM height images of a–c) fresh and d–f) thermal-aged ETL surface based on (a,d) bare ZnO, (b,e) ZnO/SAR, and (c,f) ZnO/OCS.

To determine the reason for the enhancement of thermal stability of OSCs with UV resins, we first analyzed the values of J_{dark} of the relevant devices; the measurement of this value can be considered a direct and unambiguous measurement of the charge recombination loss in OSCs, where recombination loss is a fundamental process determining the photovoltaic performance. The dark J - V characteristics of the OSCs before and after 200 h of thermal aging were measured, as shown in Figure 6c. Notably, the large variation in J_{dark} of the bare ZnO-based OSCs before and after thermal degradation corresponded to poor thermal stability. Therefore, the observed instability of the bare ZnO ETL should be ascribed to an increased interfacial charge recombination rate and substantial concomitant dark saturation current. Conversely, minor variations can be seen in the values of J_{dark} of OSCs based on UV resin modification; compared to control device, J_{dark} values are lower by orders of magnitude and there is a larger rectification ratio. It is worth mentioning that the subtle change in $J_{\text{dark}}-V$ characteristics of OSCs based on modified ZnO ETLs under thermal stress is one of the reasons for the improved thermal stability.

To further establish reasons for the different thermal stabilities of OSCs induced by ETLs, we monitored changes in water contact angles (WCAs) and surface roughness of ETLs before and after thermal stress at 120 °C for 3 h. The WCAs of the ETLs subjected to thermal stress (Figure S14, Supporting Information) were compared to those of the fresh films (Figure S2, Supporting Information). The ZnO films modified with SAR or OCS resins exhibited negligible changes in WCA values (0.3° and 0.6° for ZnO/SAR and ZnO/OCS, respectively), while pristine ZnO ETL showed an obvious change (4.8°) upon thermal stress. In the atomic force microscopy (AFM) analysis (Figure 7), a similar trend was observed in the surface roughness of ETLs:

neat ZnO film showed a larger change (0.36 nm) in surface roughness after 3 h of thermal aging at 120 °C. On the contrary, morphologies of ZnO surfaces with the modification of UV resins were not significantly altered under thermal stress, with RMS values slightly decreasing from 2.49 to 2.42 nm for ZnO/SAR and from 2.28 to 2.25 nm for ZnO/OCS. Both the WCA and AFM results indicate that the ZnO surface with SAR or OCS resins formed a robust and firmly crosslinked network that was highly resistant to thermal stress. More importantly, both light soaking and thermal stability of OSCs remarkably improved after modifying ZnO ETL with UV resins.

3. Conclusion

In summary, we have developed a simple and effective approach to enhancing the efficiency and stability of inverted OSCs utilizing SAR and OCS UV resins for modification of the ZnO/PM6:Y6-BO interface. Our findings reveal that crosslinked SAR or OCS on ZnO led to higher solvent resistance, upshifted WF, suppressed surface defects, and reduced surface energy. Utilizing ZnO/SAR and ZnO/OCS ETL, a remarkable PCE of 16.1% was attained in inverted OSCs based on PM6:Y6-BO photoactive system. Notably, the photocatalytic activity of ZnO, which decomposes Y6-BO under UV irradiation, was substantially mitigated by SAR or OCS interfacial modification. As a result, OSCs based on SAR or OCS resins retained over 80% of their initial values of PCE, while the control OSC maintained 56% of its initial efficiency after light soaking for 1000 h. Similarly, OSCs with ZnO/SAR and ZnO/OCS ETL retained 73% and 78% of their initial PCE values under thermal stress at 120 °C for 200 h, whereas neat ZnO-based OSCs retained only 58% of their initial

PCE values. This work successfully addresses and tackles the instability problem of inverted OSCs; the key findings pave the way for upscaling of these devices and, perhaps, of related organic electronic devices.

Supporting Information

Supporting Information is available from the Wiley Online Library or from the author.

Acknowledgements

The authors would like to acknowledge Partnership for Skills in Applied Sciences, Engineering and Technology (PASET)-Regional Scholarship Innovation Fund (RSIF) (World Bank PASET No. IP22-15). This work was also supported by the National Research Foundation (NRF) (NRF-2021R1A2C2091787 and NRF-2022M3H4A1A03076280) and by the National Research Council of Science and Technology (grant no. Global-23-007) of Republic of Korea. The authors are grateful to Special Materials Source (SMS) Company, Republic of Korea, for supplying the SAR and OCS UV resins.

Conflict of Interest

The authors declare no conflict of interest.

Data Availability Statement

The data that support the findings of this study are available from the corresponding author upon reasonable request.

Keywords

crosslinked UV resins, light-soaking stabilities, organic solar cells, thermal stabilities, zinc oxide modifications

Received: September 27, 2023

Revised: January 2, 2024

Published online:

- [1] J. Fu, P. W. K. Fong, H. Liu, C.-S. Huang, X. Lu, S. Lu, M. Abdelsamie, T. Kodalle, C. M. Sutter-Fella, Y. Yang, G. Li, *Nat. Commun.* **2023**, *14*, 1760.
- [2] S. Li, C. He, T. Chen, J. Zheng, R. Sun, J. Fang, Y. Chen, Y. Pan, K. Yan, C.-Z. Li, M. Shi, L. Zuo, C.-Q. Ma, J. Min, Y. Liu, H. Chen, *Energy Environ. Sci.* **2023**, *16*, 2262.
- [3] Q. Fan, R. Ma, Z. Bi, X. Liao, B. Wu, S. Zhang, W. Su, J. Fang, C. Zhao, C. Yan, K. Chen, Y. Li, C. Gao, G. Li, W. Ma, *Adv. Funct. Mater.* **2023**, *33*, 2211385.
- [4] P. Cheng, X. Zhan, *Chem. Soc. Rev.* **2016**, *45*, 2544.
- [5] S. Rafique, S. M. Abdullah, K. Sulaiman, M. Iwamoto, *Renewable Sustainable Energy Rev.* **2018**, *84*, 43.
- [6] X. Xu, D. Li, J. Yuan, Y. Zhou, Y. Zou, *EnergyChem* **2021**, *3*, 10004.
- [7] W. Liu, J. Yuan, C. Zhu, Q. Wei, S. Liang, H. Zhang, G. Zheng, Y. Hu, L. Meng, F. Gao, Y. Li, Y. Zou, *Sci. China Chem.* **2022**, *65*, 1374.
- [8] B. Liu, H. Sun, J. W. Lee, Z. Jiang, J. Qiao, J. Wang, J. Yang, K. Feng, Q. Liao, M. An, B. Li, D. Han, B. Xu, H. Lian, L. Niu, B. J. Kim, X. Guo, *Nat. Commun.* **2023**, *14*, 967.
- [9] M. Chang, L. Meng, Y. Wang, X. Ke, Y.-Q.-Q. Yi, N. Zheng, W. Zheng, Z. Xie, M. Zhang, Y. Yi, H. Zhang, X. Wan, C. Li, Y. Chen, *Chem. Mater.* **2020**, *32*, 2593.
- [10] Y. Jiang, X. Dong, L. Sun, T. Liu, F. Qin, C. Xie, P. Jiang, L. Hu, X. Lu, X. Zhou, W. Meng, N. Li, C. J. Brabec, Y. Zhou, *Nat. Energy* **2022**, *7*, 352.
- [11] N. Ahmad, H. Zhou, P. Fan, G. Liang, *EcoMat* **2021**, *4*, e12156.
- [12] Y. Wang, Z. Zheng, J. Wang, X. Liu, J. Ren, C. An, S. Zhang, J. Hou, *Adv. Mater.* **2023**, *35*, 2208305.
- [13] L. Di Mario, D. G. Romero, H. Wang, E. K. Tekelenburg, S. Meems, T. Zaharia, M. A. Loi, *Adv. Mater.* **2023**, 2301404, 10.1002/adma.202301404.
- [14] K. Zhang, Z. Hu, R. Xu, X.-F. Jiang, H.-L. Yip, F. Huang, Y. Cao, *Adv. Mater.* **2015**, *27*, 3607.
- [15] J. Yao, B. Qiu, Z.-G. Zhang, L. Xue, R. Wang, C. Zhang, S. Chen, Q. Zhou, C. Sun, C. Yang, M. Xiao, L. Meng, Y. Li, *Nat. Commun.* **2020**, *11*, 2726.
- [16] H. Nie, M. Busireddy, H.-M. Shih, C.-W. Ko, J.-T. Chen, C.-C. Chang, C.-S. Hsu, *ACS Appl. Mater. Interfaces* **2022**, *15*, 1718.
- [17] C. Liu, C. Xiao, W. Li, *J. Mater. Chem. C* **2021**, *9*, 14093.
- [18] Z. Liang, Q. Zhang, L. Jiang, G. Cao, *Energy Environ. Sci.* **2015**, *8*, 3442.
- [19] P. Cai, X. F. Huang, T. Zhan, G. T. Chen, R. H. Qiu, L. J. Zhang, X. G. Xue, Z. M. Wang, J. W. Chen, *ACS Appl. Mater. Interfaces* **2021**, *13*, 12296.
- [20] S. Li, Z. Xiao, J. J. Li, Z. Y. Hu, Y. Yang, B. Khan, D. S. Guo, X. Wan, Z. Yao, C. Li, Y. Chen, *Sci. China Chem.* **2023**, *66*, 195.
- [21] M. Günther, S. Lotfi, S. S. Rivas, D. Blätte, J. P. Hofmann, T. Bein, T. Ameri, *Adv. Funct. Mater.* **2023**, *33*, 2209768.
- [22] C. B. Ong, L. Y. Ng, A. W. Mohammad, *Renewable Sustainable Energy Rev.* **2018**, *81*, 536.
- [23] Y. Jiang, L. Sun, F. Jiang, C. Xie, L. Hu, X. Dong, F. Qin, T. Liu, L. Hu, X. Jiang, Y. Zhou, *Mater. Horiz.* **2019**, *6*, 1438.
- [24] A. Soultati, A. Verykios, S. Panagiotakis, K.-K. Armadorou, M. I. Haider, A. Kaltzoglou, C. Drivas, A. Fakharuddin, X. Bao, C. Yang, A. R. B. M. Yusoff, E. K. Evangelou, L. Petsalakis, S. Kennou, P. Falaras, K. Yannakopoulou, G. Pistolis, P. Argitis, M. Vasilopoulou, *ACS Appl. Mater. Interfaces* **2020**, *12*, 21961.
- [25] M. Gunther, D. Blatte, A. L. Oechsle, S. S. Rivas, A. A. Yousefi Amin, P. Muller-Buschbaum, T. Bein, T. Ameri, *ACS Appl. Mater. Interfaces* **2021**, *13*, 19072.
- [26] L. Hu, Y. Jiang, L. Sun, C. Xie, F. Qin, W. Wang, Y. Zhou, *J. Phys. Chem. Lett.* **2021**, *12*, 2607.
- [27] J. Guo, Y. Wu, R. Sun, W. Wang, J. Guo, Q. Wu, X. Tang, C. Sun, Z. Luo, K. Chang, Z. Zhang, J. Yuan, T. Li, W. Tang, E. Zhou, Z. Xiao, L. Ding, Y. Zou, X. Zhan, C. Yang, Z. Li, C. J. Brabec, Y. Li, J. Min, *J. Mater. Chem. A* **2019**, *7*, 25088.
- [28] P. Thirukumaran, R. Atchudan, A. S. Parveen, K. Kalaiarasan, Y. R. Lee, S. C. Kim, *Sci. Rep.* **2019**, *9*, 19509.
- [29] Y. Li, T. Li, J. Wang, X. Zhan, Y. Lin, *Sci. Bull.* **2022**, *67*, 171.
- [30] J. Huang, H. Yu, X. Zhou, *Chem. Eng. J.* **2022**, *428*, 131366.
- [31] S. Yang, H. Yu, *Chem. Eng. J.* **2023**, *452*, 139658.
- [32] Y. Li, B. Huang, X. Zhang, J. Ding, Y. Zhang, L. Xiao, B. Wang, Q. Cheng, G. Huang, H. Zhang, Y. Yang, X. Qi, Q. Zheng, Y. Zhang, X. Qiu, M. Liang, H. Zhou, *Nat. Commun.* **2023**, *14*, 1241.
- [33] Y. Han, H. Dong, W. Pan, B. Liu, X. Chen, R. Huang, Z. Li, F. Li, Q. Luo, J. Zhang, Z. Wei, C. Q. Ma, *ACS Appl. Mater. Interfaces* **2021**, *13*, 17869.
- [34] Y. Yang, J. Wang, Y. Zu, Q. Liao, S. Zhang, Z. Zheng, B. Xu, J. Hou, *Joule* **2023**, *7*, 545.
- [35] L. Y. Su, H. H. Huang, C. E. Tsai, C. H. Hou, J. J. Shyue, C. H. Lu, C. W. Pao, M. H. Yu, L. Wang, C. C. Chueh, *Small* **2022**, *18*, 2107834.
- [36] Y. Liu, D. Zhang, G. Yang, R. Wang, J. Yu, *ACS Appl. Mater. Interfaces* **2022**, *14*, 36910.

- [37] J. Wan, R. Wen, Y. Xia, M. Dai, H. Huang, L. Xue, Z. Zhang, J. Fang, K. N. Hui, X. Fan, *J. Mater. Chem. A* **2021**, *9*, 5425.
- [38] H. Li, L. Guo, X. Liu, T. Sun, Q. Li, F. Zhang, G. Xiao, T. Fu, Y. Chen, *Front. Mater.* **2020**, *7*, 113.
- [39] Z. Abbas, S. U. Ryu, M. Haris, C. E. Song, H. K. Lee, S. K. Lee, W. S. Shin, T. Park, J.-C. Lee, *Nano Energy* **2022**, *101*, 107574.
- [40] F. C. Krebs, K. O. Sylvester-Hvid, M. Jørgensen, *Prog. Photovoltaics* **2011**, *19*, 97.
- [41] M. M. Rahman, *Polymers* **2020**, *12*, 1535.
- [42] G. Jayalakshmi, K. Saravanan, T. Balasubramanian, *J. Lumin.* **2013**, *140*, 21.
- [43] B. R. Lee, E. D. Jung, Y. S. Nam, M. Jung, J. S. Park, S. Lee, H. Choi, S. J. Ko, N. R. Shin, Y. K. Kim, S. O. Kim, J. Y. Kim, H. J. Shin, S. Cho, M. H. Song, *Adv. Mater.* **2014**, *26*, 494.
- [44] Z. Ma, Y. Dong, Y. J. Su, R. Yu, H. Gao, Y. Gong, Z. Y. Lee, C. Yang, C. S. Hsu, Z. Tan, *ACS Appl. Mater. Interfaces* **2022**, *14*, 1187.
- [45] J. Wang, K. Lin, K. Zhang, X.-F. Jiang, K. Mahmood, L. Ying, F. Huang, Y. Cao, *Adv. Energy Mater.* **2016**, *6*, 1502563.
- [46] A. Rudawska, E. Jacniacka, *Int. J. Adhes. Adhes.* **2009**, *29*, 451.
- [47] X. Zhu, B. Guo, J. Fang, T. Zhai, Y. Wang, G. Li, J. Zhang, Z. Wei, S. Duhm, X. Guo, M. Zhang, Y. Li, *Org. Electron.* **2019**, *70*, 25.
- [48] L. Fan, Y. Zhang, Q. Zhang, X. Wu, J. Cheng, N. Zhang, Y. Feng, K. Sun, *Small* **2016**, *12*, 5208.
- [49] M. Ramani, S. Ponnusamy, C. Muthamizhchelvan, *Opt. Mater.* **2012**, *34*, 817.
- [50] F. Schauer, *Sol. Energy Mater. Sol. Cells* **2005**, *87*, 235.
- [51] S. Dahlström, C. Ahläng, K. Björkström, S. Forsblom, B. Granroth, K. Jansson, A. Luukkonen, M. T. Masood, J. Poulizac, S. Qudisia, M. Nyman, *AIP Adv.* **2020**, *10*, 065203.
- [52] Z. Li, D. Song, Z. Xu, B. Qiao, S. Zhao, S. Wageh, A. A. Al-Ghamdi, X. Huo, *Polymers* **2021**, *13*, 2398.
- [53] T. L. H. Mai, S. Jeong, S. Kim, S. Jung, J. Oh, Z. Sun, J. Park, S. Lee, W. Kim, C. Yang, *Adv. Funct. Mater.* **2023**, *33*, 2303386.
- [54] X. Song, Y. Song, H. Xu, S. Gao, Y. Wang, J. Li, J. Hai, W. Liu, W. Zhu, *Adv. Energy Mater.* **2023**, *13*, 2203009.